FACTORIAL DESIGN FOR MACHINING OF MICRO-HOLES IN BOROSILICATE GLASS USING ECDM

Rithwik Shankar Raj

Department of Mechanical Engineering

R V College of Engineering Bangalore, India

TABLE OF CONTENTS

Abstract

This project employs the principles of factorial design for the machining of micro-holes in borosilicate glass using an in-house experimental Electrochemical Discharge Machining (ECDM) setup. This machine has been programmed to perform the machining of non-conducting, brittle, hard, and low-machinable engineering materials. The power module has been developed using Arduino as a platform. The setup has been developed for machine components and can be controlled remotely. Sensors have been used to achieve this objective. The construction of the machine circuit is comprehensive and compact. The idea proposed in this project is to repurpose and retrofit the Electrochemical Discharge Machining setup. A power module has also been developed, and IOT has been implemented to provide live feedback on the operating conditions and facilitate remote machine control. Electrochemical Discharge Machining can be used for various applications, including microfluidics machining of non-conducting materials like glass, ceramics, etc. Microfluidic devices have wide applications in the medical and biotechnological industries. They are widely used in procedures such as flow cytometry, PCR amplification, DNA analysis, separation and manipulation of cells, and cell patterning.

Motivation

Market Motivation: Micro-machining is in high demand in the market. Electrochemical discharge machining (ECDM) is a highly efficient method for producing high-quality components, especially in biochemistry, biomedicine, and electronics.

Industrial Motivation: Electrochemical Discharge Machining can be used to machine non-conducting materials like glass, ceramics, etc. The fine speed and feed control can be used to machine workpieces and components for Micro-Electromechanical Devices (MEMS) and Microfluidics applications. Incorporating IOT can also assist in monitoring the operating conditions and can facilitate remote and indirect control of the machine.

Research Motivation: The ECDM method can be used to machine non-conducting materials like quartz, glass, composites, ceramics, etc., accurately. Microfluidics is an important research application wherein microfluidic devices can be manufactured accurately using the ECDM method.

Societal motivation: Microfluidic devices are widely applied in the medical and biotechnological industries. They are widely used in procedures such as flow cytometry, PCR amplification, DNA analysis, separation and manipulation of cells, and cell patterning.

Knowledge Motivation: During the execution of the project, students learn about Arduino-uno IDE, AF Motor library, new ping library, Infrared Sensor library, CNC codes, Toolpath Generation, Gears and machine design, thermocouple and temperature measurement libraries, use of Bluetooth modules, IOT control applications, etc.

Environmental Motivation: The ECDM method is a very effective method for machining nonconducting materials. The waste generated is very minimal and is not hazardous. It is much more efficient and less harmful to the environment than other forms of non-traditional machining operations like chemical machining.

Literature Review

References	Contribution	Scope for research work
Baoyang Jiang, Jun Ni: *Micro-machining of glass using electrochemical discharge assisted cutting*. Proceedings of the ASME 2016 International Manufacturing Science and Engineering Conference MSEC2016, June 27-July 1, 2016, Blacksburg, Virginia, USA, MSEC2016-8759.	Glass is a hard-to-machine material with vast industrial application. Electrochemical discharge machining (ECDM) is a non-traditional machining technology that has shown potential for effective glass machining. This work provides results of extensive research on the micro-machining of glass using the ECDM process and focuses on parameters such as material removal rate, surface finish, and geometric accuracy.	Micro-machining of glass using ECDM has several parameters that need to be considered. Material removal rate, surface finish, and geometric accuracy differ for various cases. The required accuracy for a workpiece can be determined by varying these parameters.
Liu Y, Zhang C, Li S, Guo C, Wei Z: *Experimental study of micro electrochemical discharge machining of ultra-clear glass with a rotating helical tool*. Processes. 2019; 7(4):195.	Experiments were conducted to investigate the machining localization of ECDM with a rotating helical tool on ultra-clear glass. This paper discussed the effects of machining parameters, including pulse voltage, duty factor, pulse frequency, and feed rate.	The pulse voltage, duty factor, pulse frequency, and feed rate are important parameters involved in machining the glass workpiece. The result of the paper can be used to set optimum values of these parameters for machining the glass workpiece in the setup.
Wansheng Zhao, Mo Chen, Weiwen Xia, Xuecheng Xi, Fuchun Zhao, Yaou Zhang: *Reconstructing CNC platform for EDM machines towards smart manufacturing*, Procedia CIRP, Volume 95, 2020, ISSN 2212-8271.	CNC is important for controlling the ECDM process. This paper gave an overview of the layout and setup of the structure of CNC for EDM	The CNC layout for the ECDM set up can be adapted from the paper. Further for automation and optimization of the CNC setup, IOT and other software components, such as Deep Learning, can be incorporated.

Chapter 1: Introduction

1.1. OVERVIEW

Electrochemical Discharge Machining (ECDM) is a complex combination of Electrochemical machining (ECM) and Electric Discharge machining (EDM). The ECDM process involves melting and chemical etching of the workpiece due to the high electrical energy discharged on the tip of the electrode during electrolysis. One is the tool electrode, which is used to produce the desired machined shape, and the other is the counter electrode or auxiliary electrode made as anode. The workpiece and counter electrode (anode) are immersed in an electrolyte solution. Electrolysis starts when a voltage is supplied by a direct current (DC) power source between the tool electrode and the counter electrode. The schematic diagram for Electrochemical Discharge Machining set up is shown below (Fig 1.1).

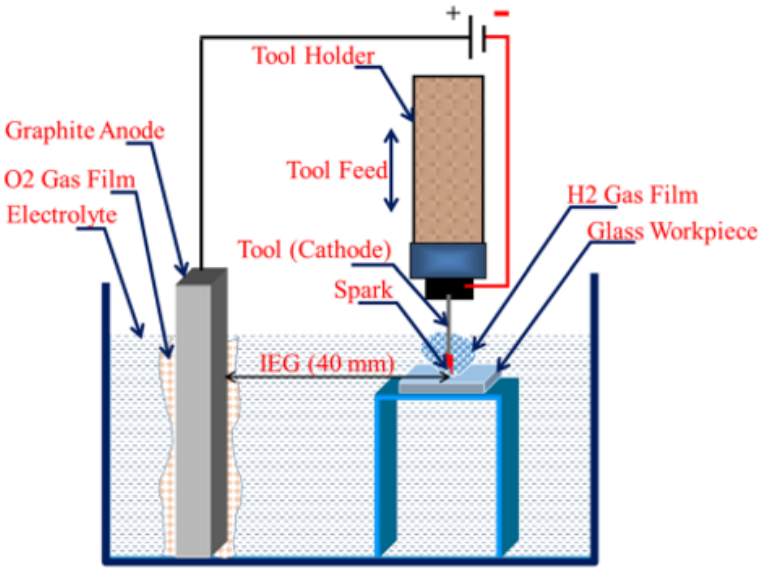

Fig 1.1 Schematic of ECDM setup

1.2. PRINCIPLE OF ELECTROCHEMICAL DISCHARGE MACHINING

The Electrochemical Discharge machining (ECDM) process combines the principles of both ECM and EDM. The tool (generally cathode) and the anode (which is very large compared to the tool diameter) are dipped in an aqueous solution of the electrolyte. When DC is applied, electrolysis takes place. The electrolytic reactions occur at the electrodes when the voltage at the inter-electrode gap of the machining zone increases beyond the required value.

Reactions at the cathode result in hydrogen production due to the chemisorption of water molecules on the electrode surface (Volmer's reaction) and by desorption either by Heyrovsky

reaction, which is an electrochemical reaction or by Tafel reaction, which is a chemical reaction.

$M + H_2O + e^- \rightarrow M\text{-}H_{ads} + OH^-$ (Volmer reaction)

$M\text{-}H_{ads} + M + H_2O + e^- \rightarrow 2M + H_2 + OH^-$ (Heyrovsky reaction)

$M\text{-}H_{ads} + M\text{-}H_{ads} \rightarrow 2M + H_2$ (Tafel reaction)

The reactions at the anode for oxygen evolution

$2H_2O \rightarrow O_2 + 4H^+ + 4e^-$ (Acidic electrolyte solution)

$4OH^- \rightarrow O_2 + 2H_2O + 4e^-$ (Alkaline electrolyte solution)

When the voltage is increased, owing to the small dimension of the tool compared to the anode, the current density at the tooltip increases, leading to the formation of a bubble layer around the electrode. When critical voltage is reached, the bubbles coalesce into a gas film around the tool electrode. When sufficient potential difference is created between the gas film and the gas-film-electrode interface, electrical discharges occur between the interfaces.

The voltage-current characteristics of water decomposition, which directly relate to the discharge phenomenon, are shown in Fig 1.2.

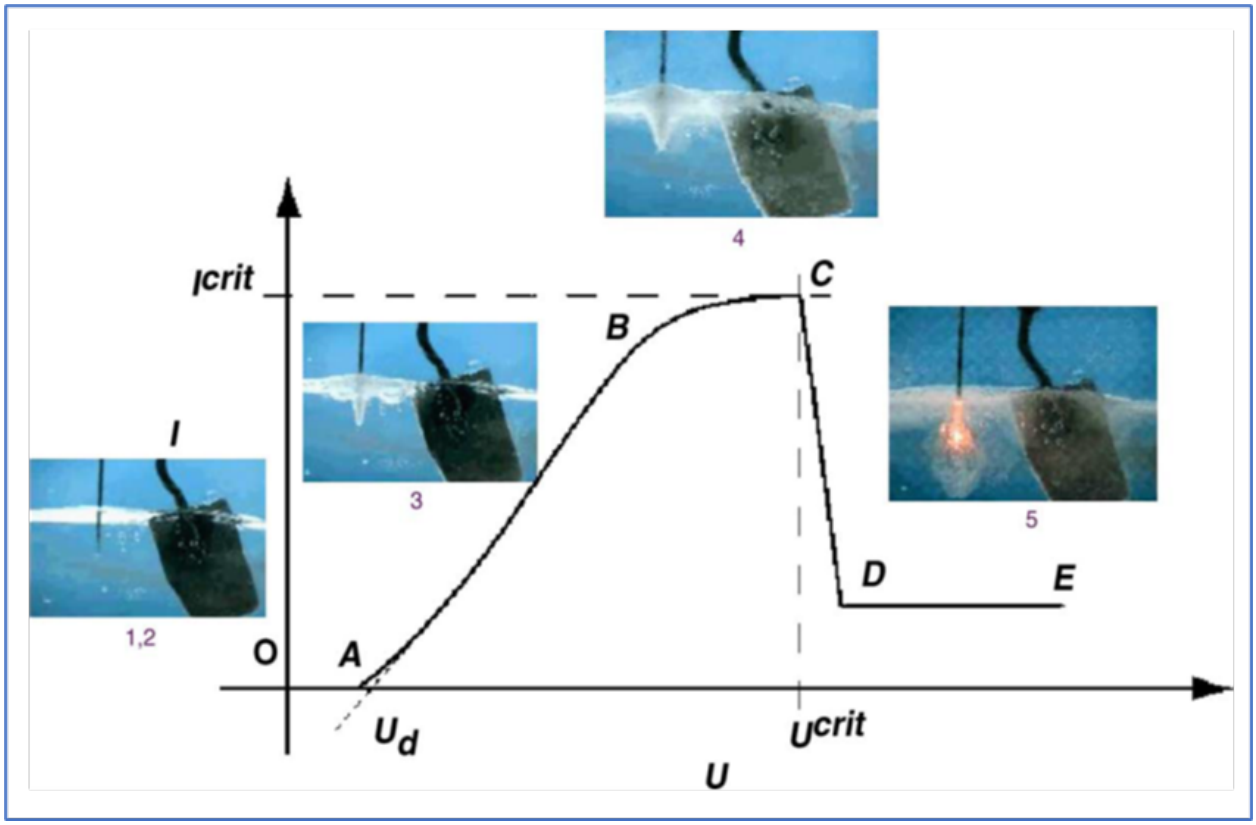

Fig 1.2 V-I characteristics of spark discharge

The electrochemical discharge is classified into five regions based on the stationary current:

i. Thermodynamic and over-potential Region:

Here, the voltage supplied is less than the decomposition potential V_d. Hence, no current flows between the electrolytes, and no significant electrolysis occurs.

ii. Ohmic region AB:

As voltage is increased, current increases nearly linearly with it. The decomposition of water into hydrogen and oxygen starts, leading to the evolution of bubbles and the beginning of the formation of the bubble layer.

iii. Limiting current region BC:

The limiting mean current value, I, is reached and almost constant in this region. Bubbles start evolving in larger sizes, and the bubble layer is formed. The limiting current region ends when the voltage reaches V_{crit}.

iv. Instability region CD:

Beyond critical voltage $V_{crit,}$ the current drops very rapidly with an increase in terminal current. A gas film surrounds the working electrode, and the electrolyte resistance diverges.

v. Electrochemical discharge region DE:

Due to the formation of the gas film, the working electrode is completely isolated from the electrolyte. Electrochemical discharges take place through the gas film and are used for machining.

1.3. MECHANISM OF MATERIAL REMOVAL FOR GLASS

During electrochemical discharge machining of borosilicate glass, sublimation of the glass surface occurs, leading to the etching of a majority of the surface by OH^- radicals, reduction in viscosity of glass at the zone of electrochemical discharges due to local heating, and formation of microcracks. The temperature at the machining zone is determined by:

- Spark intensity
- Movement of electrolytes in the machining zone
- Gap between the work-piece and electrode

The chemical reaction occurring with ECDM with glass workpiece and NaOH electrolyte is shown in the schematic diagram given in Fig 1.3. Sodium ions (Na^+) and Hydroxide ions (OH^-) are adsorbed on the glass surface, which leads to the breakage of the Si—O—Si bond and changes into the Si—O—Na bond. The Sodium bond (Na—O) is weaker than the Silicon bond (Si—O). Due to this, the binding force of -Na—O- in Na_2SiO_2 is weak, making the Na_2SiO_2 weak so that electrochemical discharges easily break it and are easily soluble in water. Hence, the material can be melted and machined by the thermal energy in electrochemical discharges.

The following equation represents the overall chemical reaction for the process:

$$SiO_2 + 2NaOH \rightarrow Na_2O\text{-}SiO_2 + H_2O$$

This material removal mechanism forms the basis for the micromachining of microfluidic devices on borosilicate glass substrates. The feed rate and the depth of cut must be carefully determined to ensure that cracks due to thermal stress do not occur in the substrates, especially near the Heat Affected Zone (HAZ). A very fine feed rate is preferred, and gradual increments in the depth of cut are necessary to maintain accuracy and reduce deviation during the machining process.

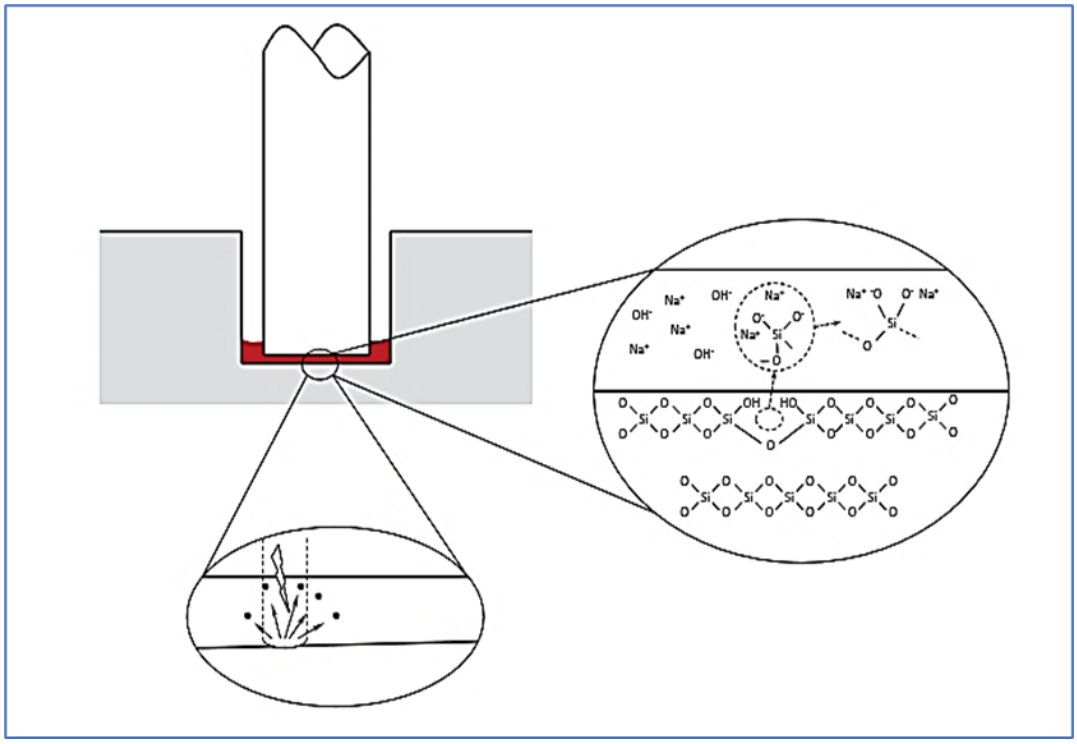

Fig 1.3 Schematic of machining mechanism with glass

1.4. REVIEW OF GLASS-BASED MICROFLUIDIC DEVICES

Glass microfluidic devices are small-scale fluidic systems fabricated using glass as the primary material. These devices are designed to manipulate and control tiny amounts of fluids, typically in the microliter or nanolitre range, for various applications in fields such as chemistry, biology, and medicine. Integrating microfluidics into glass substrates offers several advantages, including optical transparency, biocompatibility, and chemical inertness. The major difficulties occur due to the fabrication complexity, machining cost, and the material's brittleness (which can be a limitation in certain applications).

Borosilicate glass is commonly used because of its superior optical and chemical properties. The transparency of borosilicate glass is especially advantageous for optical observation and analysis. Fabrication of glass microfluidic devices is a complex process. In addition to Electrochemical Discharge Machining (ECDM), the following methods are also used for machining microfluidic devices:

- Etching: Chemical or dry etching are used to create microstructures and channels on the substrate surface. Wet etching with hydrochloric acid is also employed for glass

- Photolithography: This is a commonly used method that involves coating the glass substrate with photosensitive material, exposing it to light through a mask, and subsequently developing the pattern.

Several designs and structures can be machined on the device, such as

- Microchannels: These are small channels etched or formed on the glass substrate, typically with widths and depths in the micrometer range. These channels guide the flow of fluids within the device.
- Reservoirs and wells: Depressions or open areas are created on the substrate for sample storage and loading.
- Valves and pumps: Pneumatic or electrostatic valves can be used to enable precise fluid control using external pressure sources or electrical signals to manipulate these valves.

The microfluidic devices can also be integrated with other technologies, such as Optical Detection Systems and Lab-on-a-Chip devices, where several analytical processes are integrated into a single device.

Chapter 2: Development Of Circuits and Initial Setup

2.1. OVERVIEW OF COMPONENTS USED

2.1.1. Arduino Uno:

Arduino UNO is a microcontroller board based on the ATmega328P, as shown in Fig 2.1. It has 14 digital input/output pins (of which six can be used as PWM outputs), six analog inputs, a 16 MHz ceramic resonator, a USB connection, a power jack, an ICSP header, and a reset button.

Fig 2.1 Arduino UNO ATmega328P

2.1.2. Node MCU:

The NodeMCU ESP8266 development board comes with the ESP-12E module containing the ESP8266 chip having Tensilica Xtensa 32-bit LX106 RISC microprocessor, as shown in Fig 2.2. This microprocessor supports RTOS and operates at 80MHz to 160 MHz adjustable clock frequency. NodeMCU has 128 KB RAM and 4MB of Flash memory to store data and programs. Its high processing power with in-built Wi-Fi / Bluetooth and Deep Sleep Operating features make it ideal for IoT projects.

NodeMCU can be powered using a Micro USB jack and VIN pin (External Supply Pin). It supports UART, SPI, and I2C interfaces.

Fig 2.2 Node MCU

2.1.3. Stepper Motors:

NEMA 17 is a hybrid stepping motor with a 1.8° step angle (200 steps/revolution), as shown in Fig 2.3. Each phase draws 1.2 A at 4 V, allowing for a holding torque of 3.2 kg-cm. NEMA 17 Stepper motor is generally used in Printers, CNC machines, and Laser Cutters.

This motor has six wires connected to two split windings. While Black, Yellow, and Green wires are part of the first winding, Red, White, and Blue are part of the second winding.

Fig 2.3 NEMA-17 Stepper Motor

2.1.4. Thermocouple (MAX 6675):

The MAX6675 performs cold-junction compensation and digitizes the signal from a type-K thermocouple. The data is output in a 12-bit resolution, SPI-compatible, read-only format, as shown in Fig 2.4. This converter resolves

temperatures to 0.25°C, allows readings as high as +1024°C, and exhibits thermocouple accuracy of 8 LSBs for temperatures ranging from 0°C to +700°C. The MAX6675 is available in a small, 8-pin SO package

Fig 2.4 MAX 6675 cold junction thermocouple

2.1.5. 20 × 4 LCD Display:

This is a 20×4 Arduino-compatible LCD display module with a high-speed I2C interface, as shown in Fig 2.5. It can display 20×4 characters on two lines of white characters on a blue background. This I2C 20×4 LCD display module is designed for Arduino microcontroller. It uses an I2C communication interface, with this I2C interface, only two lines (I2C) are required to display the information on any Arduino-based projects. It will save at least four digital/analog pins on Arduino. All connectors are standard XH2.54 (Breadboard type).

Fig 2.5 20 × 4 LCD Display

2.1.6. DC Motor:

A DC motor is used to drive the spindle of the ECDM setup. The motor is shown in Fig 2.6.

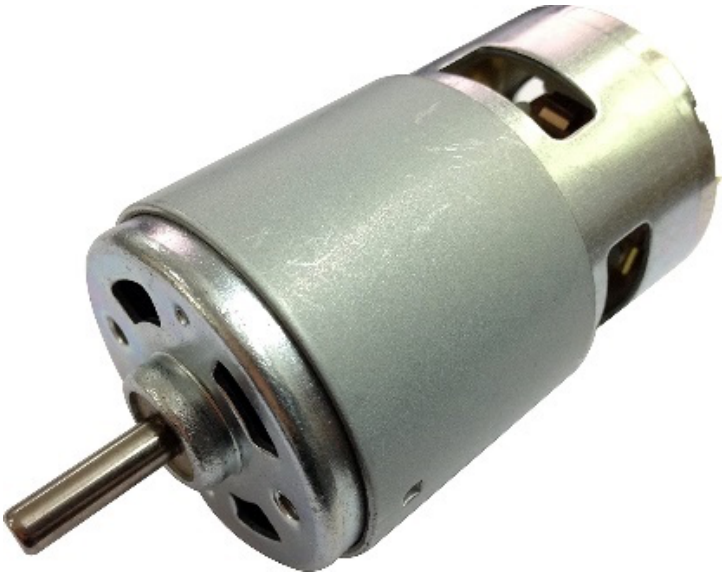

Fig 2.6 DC Motor

2.1.7. Arduino CNC Shield:

Arduino CNC shields provide an Arduino microcontroller with the power necessary to drive stepper motors and run all the other functions contributing to a CNC machine's operation, as shown in Fig 2.7. Depending on the shield, this could include end stops, spindle speed control, and probing. It utilizes an Arduino Uno and requires a 12–36-volt power supply to drive the motors. It runs the common GRBL Arduino CNC firmware. It can support up to four plug-in stepper motor drivers, and this shield can clone an axis.

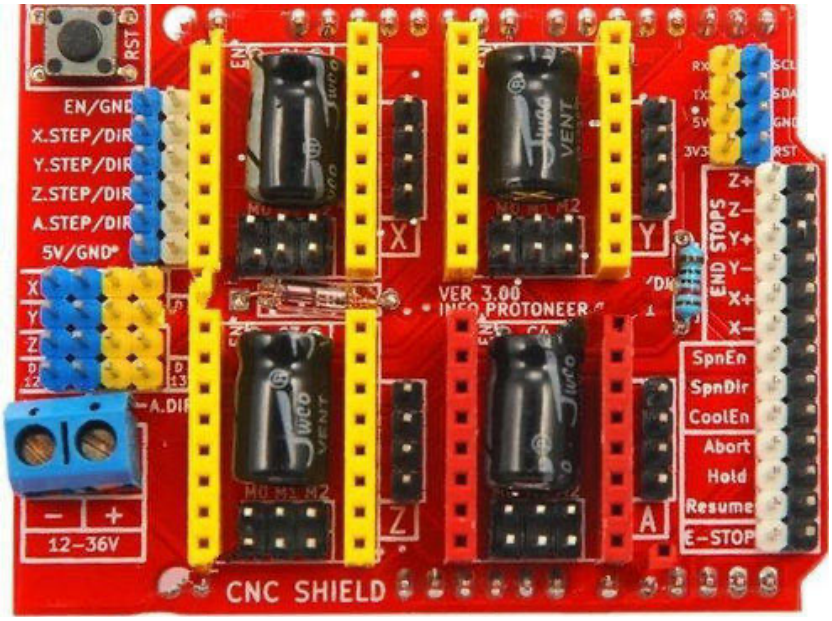

Fig 2.7 Arduino GRBL CNC Shield

2.1.8. Bluetooth Module (hc05):

HC-05 Bluetooth Module is an easy-to-use Bluetooth SPP (Serial Port Protocol) module designed for transparent wireless serial connection setup, as shown in Fig 2.8. Its communication is via serial communication, making it easy to interface with a controller or PC. HC-05 Bluetooth module provides a switching mode between master and slave mode, which means it can use neither receiving nor transmitting data.

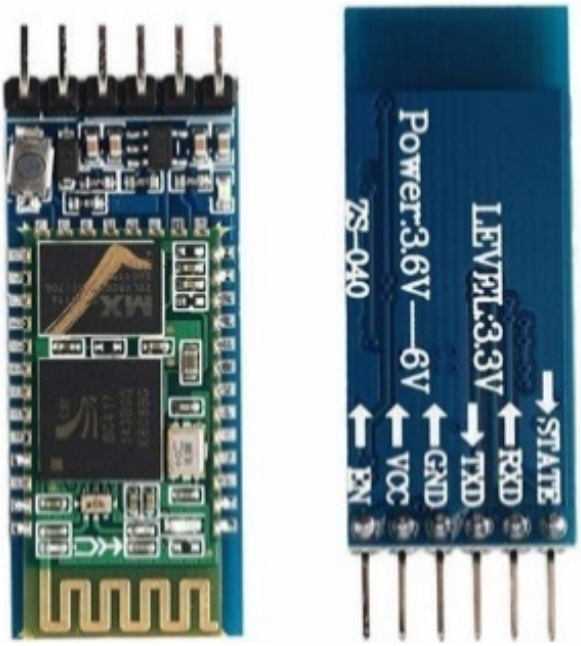

Fig 2.8 hc05 Bluetooth module

2.1.9. Cooling Fan:

The cooling fan removes the heat generated in the power module setup. The fan is shown in Fig 2.9.

Fig 2.9 Computer cooling fan

2.1.10. IR Sensors:

The IR sensor was used to calculate the spindle's rotation speed (Fig 2.10). The speed of the shaft is measured in RPM and is displayed on the LCD display.

Fig 2.10 IR Sensor

2.1.11. Joystick:

A joystick has been used to control the movement along the vertical axis (Fig 2.11).

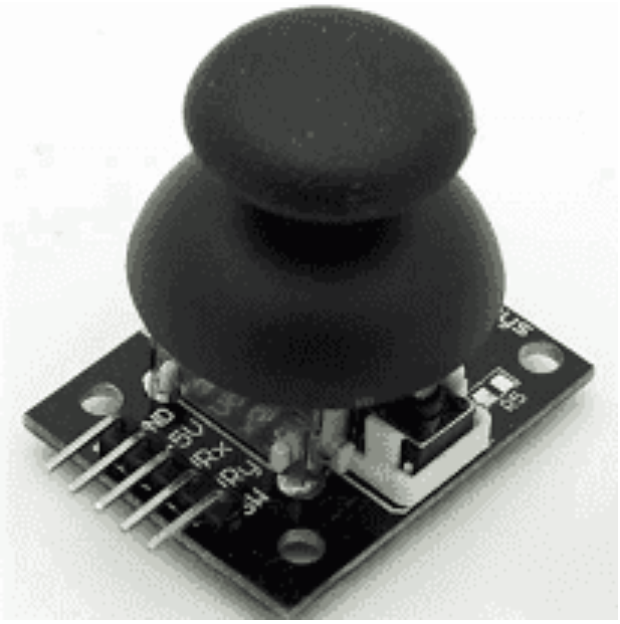

Fig 2.11 Joystick

2.1.12. Potentiometer:

A potentiometer is used to control the spindle's rotational speed as shown in Fig. 2.12.

Fig 2.12 Rotary potentiometer control

Chapter 3: Experimental Setup

3.1. SPECIFICATION OF COMPONENTS

3.1.1. Specifications of NEMA-17 Stepper Motor

- Rated Voltage: 12V DC
- Current: 1.2A at 4V
- Step Angle: 1.8 deg.
- No. of Phases: 4
- Motor Length: 1.54 inches
- 4-wire, 8 inch lead
- 200 steps per revolution, 1.8 degrees
- Operating Temperature: -10 to 40 °C
- Unipolar Holding Torque: 22.2 oz-in

3.1.2. Specifications of Node MCU

- Microcontroller: Tensilica 32-bit RISC CPU Xtensa LX106
- Operating Voltage: 3.3V
- Input Voltage: 7-12V
- Digital I/O Pins (DIO): 16
- Analog Input Pins (ADC): 1
- UARTs: 1
- SPIs: 1
- I2Cs: 1

- Flash Memory: 4 MB
- SRAM: 64 KB
- Clock Speed: 80 MHz
- USB-TTL based on CP2102 is included onboard, Enabling Plug n Play
- PCB Antenna

3.1.3. Specifications of Bluetooth Module (hc05)

- Serial Bluetooth module for Arduino and other microcontrollers
- Operating Voltage: 4V to 6V (Typically +5V)
- Operating Current: 30mA
- Range: <100m
- Works with Serial communication (USART) and TTL compatible
- Follows IEEE 802.15.1 standardized protocol
- Uses Frequency-Hopping Spread spectrum (FHSS)
- Can operate in Master, Slave or Master/Slave mode

3.1.4. Specifications of Arduino Uno

- Rated Voltage: 3~6V
- Continuous No-Load Current: 150mA +/- 10%
- Min. Operating Speed (3V): 90+/- 10% RPM
- Min. Operating Speed (6V): 200+/- 10% RPM
- Torque: 0.15Nm ~0.60Nm
- Body Dimensions: 70 x 22 x 18mm

- Weight: 30.6g

3.2. CIRCUIT DIAGRAMS AND SCHEMATICS

The circuit diagram for the ECDM setup is shown in Fig 3.1. The working table is mounted on the X-stage motor. The working table is thus capable of moving horizontally with the workpiece. The main motor is responsible for the vertical movement (Y-stage). The stepper motor mounted is responsible for finely controlling the feed rate, which is essential for the micro-machining of the glass workpiece. A high-speed motor is responsible for the rotation of the spindle. The support base supports the entire setup and absorbs the moving components' residual vibrations.

3.2.1. Schematic of ECDM setup

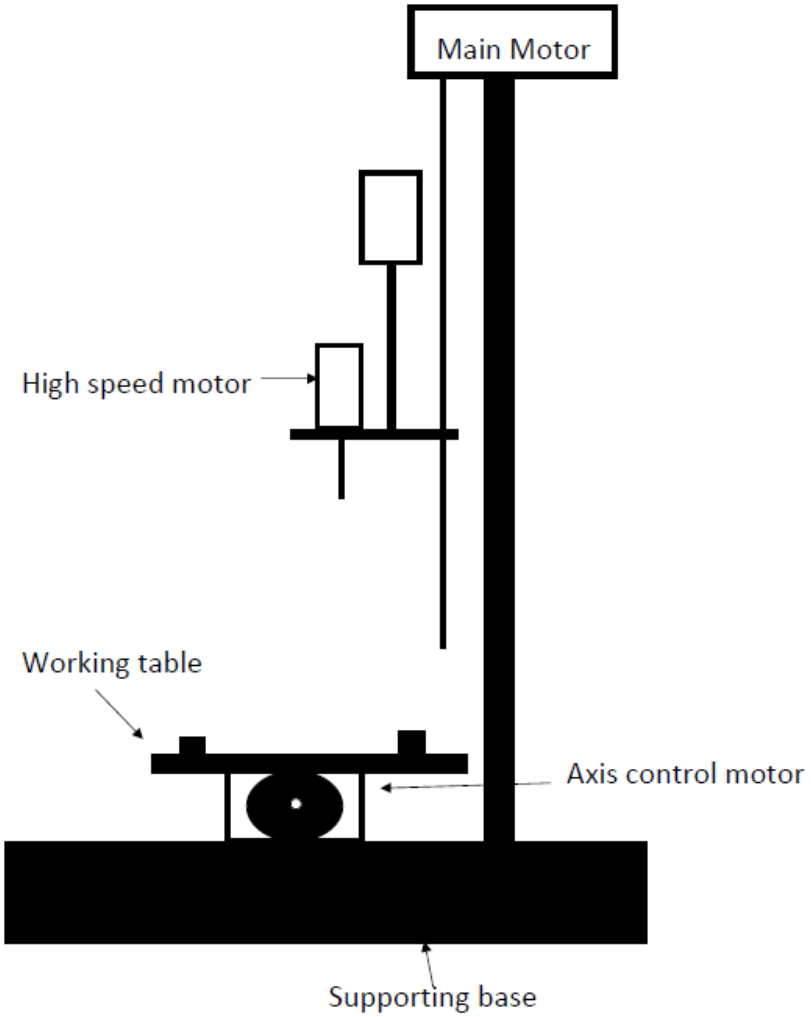

Fig 3.1 Schematic of ECDM setup

The schematic for the ECD test rig is shown in Fig 3.2. The tool electrode is the cathode, and the Auxiliary electrode acts as the anode. A 5V DC power source is used. The transistor and MOSFET are used to generate pulse frequency for the spark during the machining of the component. The waveform can be visualized using an oscilloscope.

3.2.2. Layout of ECDM Test Rig

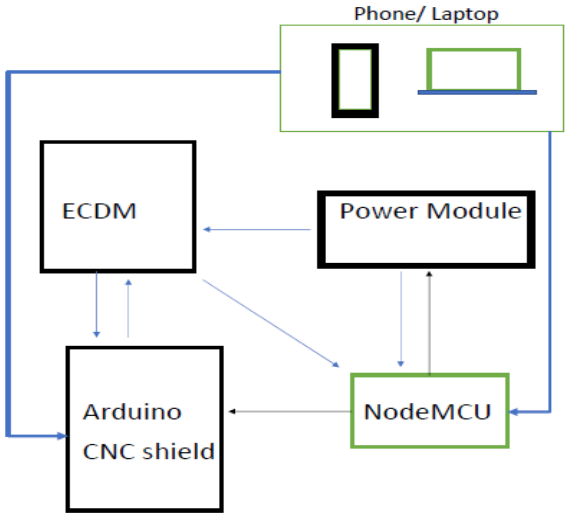

Fig 3.2 Layout of ECDM test rig

3.2.3. Power module for ECDM

The MOSFET IRF540 is a switch for turning the high voltage and high current power on and off at the desired frequency. This is shown in Fig 3.3.

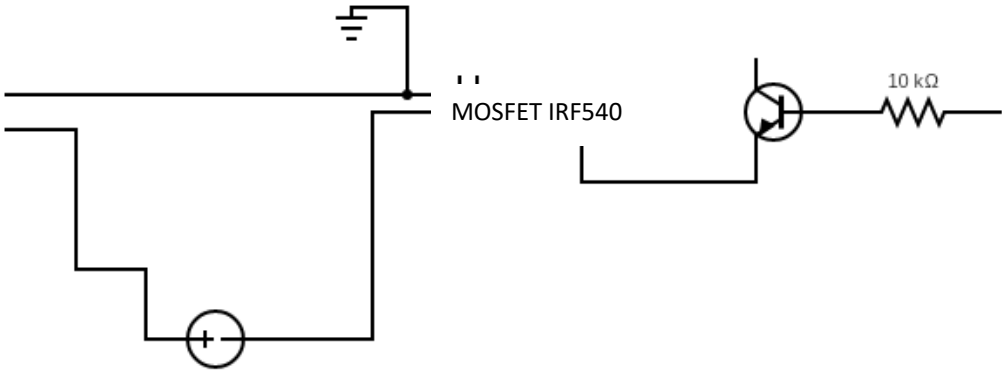

Fig 3.3 Power Module for ECDM

3.2.4. GRBL Controller Circuit

The circuit to control the stepper motors and to facilitate the uploading and running of G-Codes using the GRBL controller is shown in Fig 3.4.

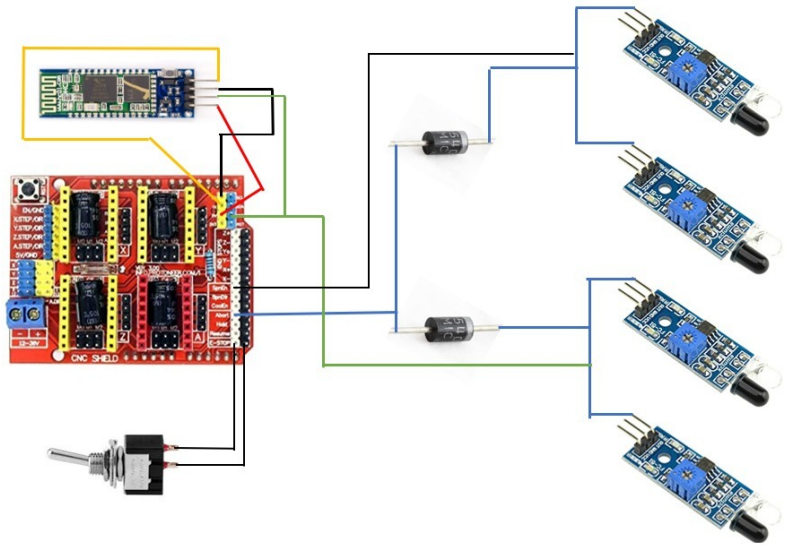

Fig 3.4 GRBL controller circuit (CNC Shield)

3.2.5. Main Z-Axis Controller Circuit

The circuit to control the main Z-Axis is shown in Fig 3.5.

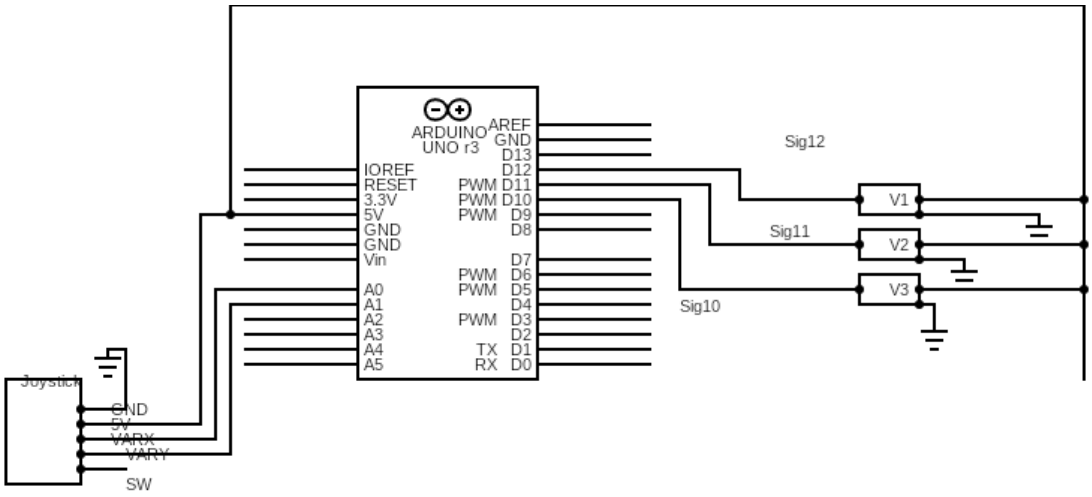

Fig 3.5 MAIN Z AXIS CONTROLLER CIRCUIT

3.2.6. Frequency generation circuit

The frequency generation circuit is shown in Fig 3.6.

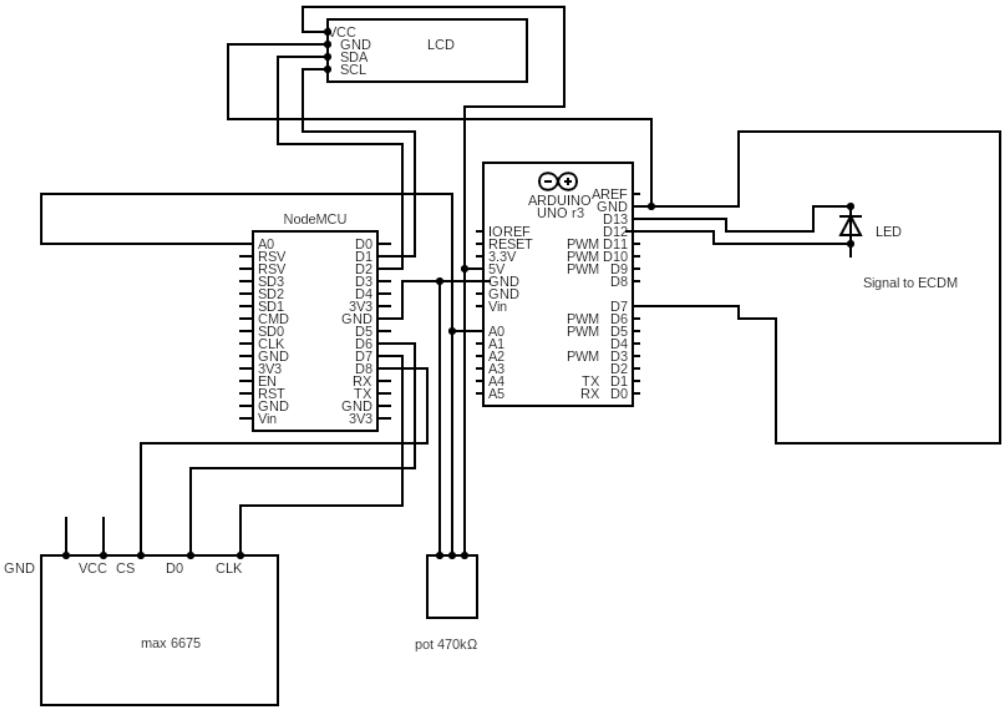

Fig 3.6 Frequency generation circuit

3.3. SOFTWARES AND LIBRARIES USED:

3.3.1. Arduino IDE

For coding and for uploading the code in Arduino-Uno.

3.3.2. New Ping Library

A library that makes working with ultrasonic sensors easy.

3.3.3. HCSR04 Library

Allows Arduino board to use the HCSR04 model to get the current distance in cm.

3.3.4. AF Motor Library

Provides speed and direction control for up to four DC motors when used with a motor shield.

3.4. ASSEMBLING AND TESTING OF PARTS AND COMPONENTS

The parts and components of the circuit and the machine have been assembled in several stages, as mentioned below. After completing the assembly process, several tests have been carried out with different feeds and speeds. The tests were carried out on glass workpieces.

3.4.1. Building Circuit for Motion Control

The circuit for motion control is shown in Fig 3.7. This circuit moves the X and Y stages and the spindle rotation. The code has been uploaded to the Arduino boards.

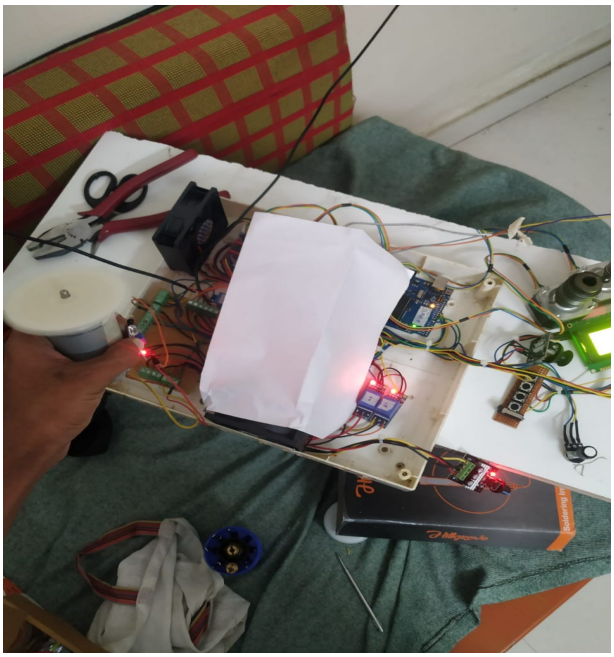

Figure 3.7 Building circuit for motion control

3.4.2. Fabrication of Motion Control and ECDM Circuits

The fabrication of circuits for motion control and the ECDM process is shown in Fig 3.8 and Fig 3.9. The cooling fan is necessary to remove the heat developed in the circuit environment during machining. The parameters that can be displayed are pulse frequency, spindle speed, and the circuit housing temperature.

The control of motion of the different stages and the spindle speed can be controlled indirectly from a mobile phone.

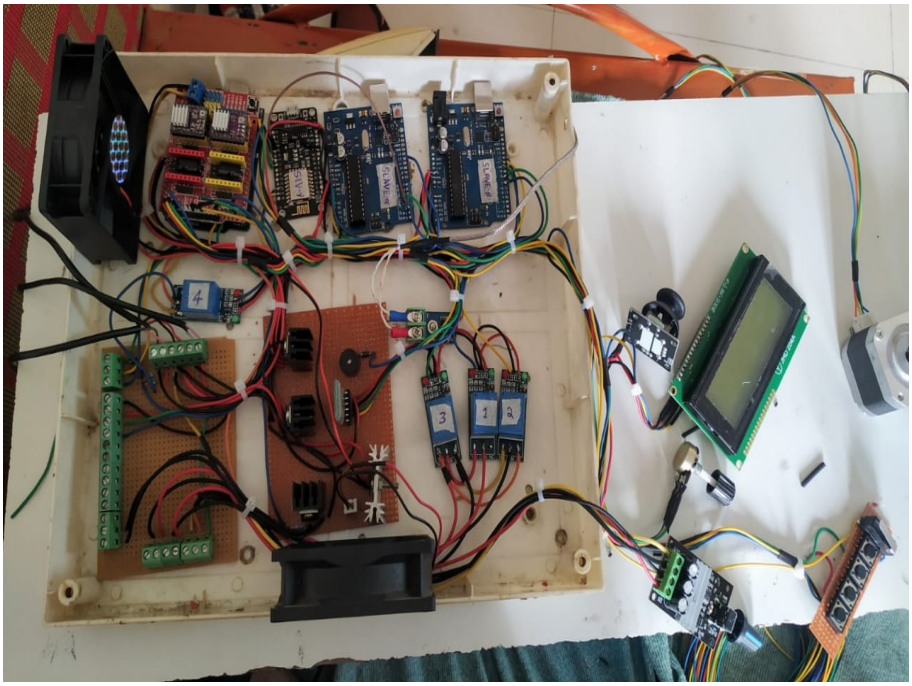

Fig 3.8 Fabricating motion control circuit

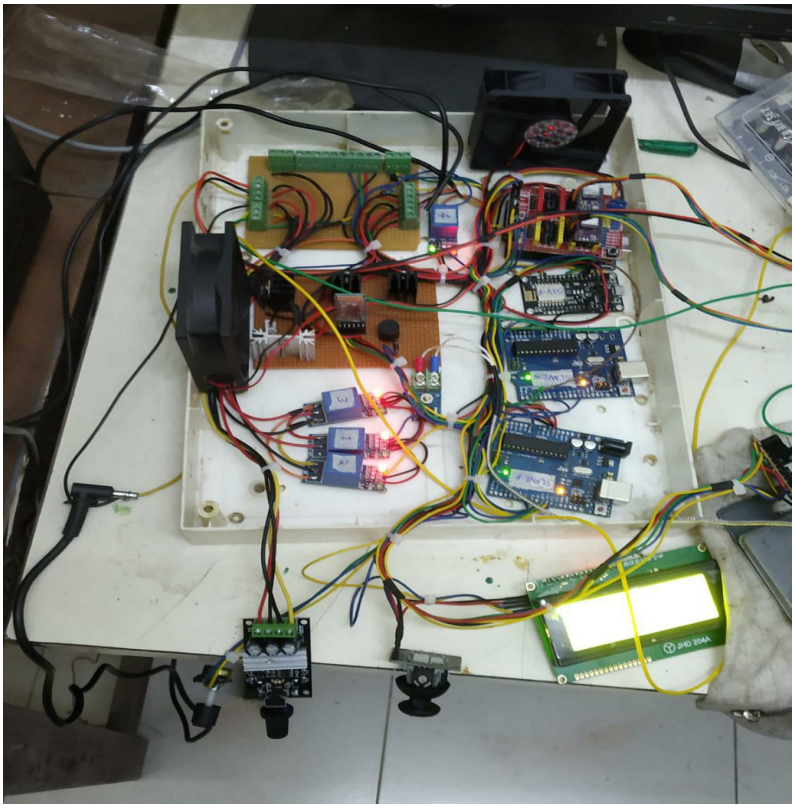

Fig 3.9 Fabricated circuit for both motion control and ECDM process

3.4.3. Testing of ECDM Process

The testing of the ECDM process is shown in Fig 3.10 and Fig 3.11. The workpiece used is a glass workpiece. The testing phase aims to validate the circuitry development for the power module and IOT control. Several holes have been machined on the glass surface for different speeds and feed values.

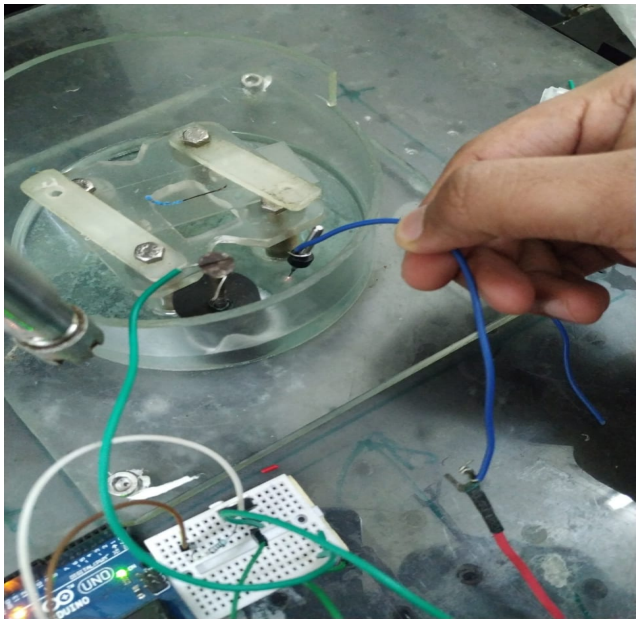

Fig 3.10 Testing of ECDM process

The LCD display displays pulse frequency, circuit housing temperature, and spindle speed process parameters, as shown in Fig 3.11.

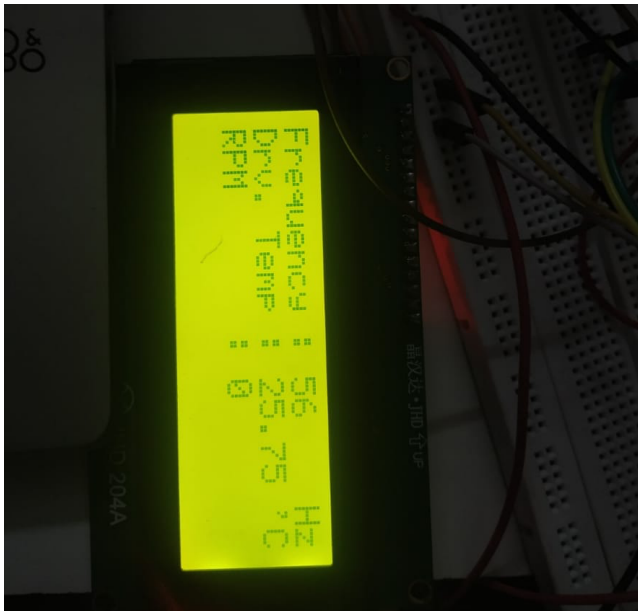

Fig 3.11 LCD display showing frequency, speed, and temperature

Chapter 4: Factorial Design using MINITAB Software

Factorial design is a research design commonly used in experimental and research studies to investigate the effects of multiple independent variables simultaneously. It is a systematic method for examining the influence of different factors and their interactions on a dependent variable. A factorial design involves manipulating two or more factors (independent variables) to observe their individual and combined effects on the dependent variable.

Factors are the independent variables manipulated in the study. Each factor can have multiple levels, representing different operating conditions or values. Levels are the specific values or conditions that each factor can take.

Some common factorial design notations are as follows:

- **2×2 Design:** A common factorial design with two factors, each with two levels.
- **3×2 Design:** A design with two factors, one with three levels and the other with two levels.
- **k×k Design:** General notation for a factorial design with k factors, each with k levels.

A 2×2 design can be denoted as 2^2, indicating two factors, each with two levels. Generalizing, a k×k design is denoted as k^k. Factorial design is a powerful and flexible research methodology that allows researchers to study the effects of multiple factors simultaneously. It provides a structured approach to understanding main effects and interactions, contributing to a more comprehensive understanding of the relationships among variables. The complexity of the design can vary, and researchers need to carefully consider factors such as the number of factors, levels, and the practical constraints of the study.

4.1. MINITAB Software for Factorial Design

Minitab is a statistical software package designed to assist professionals in statistical analysis and data visualization. It provides a user-friendly interface for statistical analysis, data manipulation, and graphical data representation. Minitab allows users to input and manipulate data efficiently. Users can enter data directly into the spreadsheet or import data from other sources such as Excel or text files. Minitab offers a wide range of statistical analyses, including descriptive statistics, hypothesis testing, regression analysis, analysis of variance (ANOVA), and non-parametric tests. It also supports specialized analyses like reliability analysis and survival analysis.

Minitab provides tools for creating various graphs and charts to represent data visually. Common graphical outputs include histograms, scatterplots, boxplots, and control charts.

These visualizations aid in understanding data distributions, trends, and patterns. Minitab is particularly well-known for its suite of quality improvement tools. It includes statistical process control (SPC) charts, capability analysis, design of experiments (DOE), and tools for Six Sigma methodologies. Minitab is used widely in industries that rely highly on quality improvement, such as manufacturing and healthcare. It is extremely important in Six Sigma initiatives, where organizations aim to achieve high quality and process efficiency levels.

A multi-level design is chosen with two levels and two factors each. Voltage and frequency are chosen as the factors. Four runs are carried out, and the ANOVA chart is generated. The plots are generated for the individual and the interaction effects of the two factors.

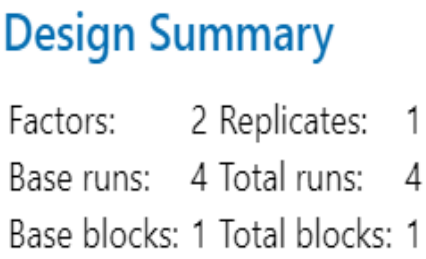

Fig 4.1 MINITAB Design Summary

The design summary is shown in Fig 4.1. The two factors chosen are spark voltage and spark frequency. For the in-house experimental setup, the voltage was assigned two levels of 30V and 60V. Similarly, the spark frequency is assigned two levels of 40Hz and 60Hz. The aim is to understand the effect of variation in Machining time with changes in voltage and frequency.

The factorial design sample values for experimental spark voltage and frequency are shown in Fig 4.2. The experimental setup's voltage regulator and spark frequency oscillator are controlled to test the voltage and frequency cases.

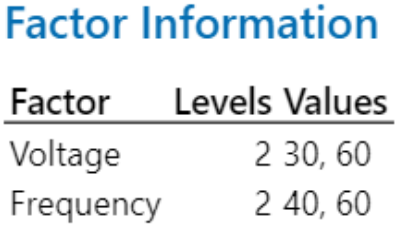

Fig 4.2 Factorial Design sample values for experimental voltage and frequency

The analysis of variance (ANOVA) table in Minitab summarizes the statistical results for the main effects and interactions in a factorial design, such as a 2×2 design. The ANOVA table

breaks down the variation in the response variable into components attributable to each factor and their interactions. The ANOVA table for the study is shown in Fig 4.3.

Analysis of Variance

Source	DF	Adj SS	Adj MS	F-Value	P-Value
Model	2	162.500	81.250	1.44	0.507
Linear	2	162.500	81.250	1.44	0.507
Voltage	1	156.250	156.250	2.78	0.344
Frequency	1	6.250	6.250	0.11	0.795
Error	1	56.250	56.250		
Total	3	218.750			

Fig 4.3 Analysis of Variance (ANOVA) table

Chapter 5: Machining of Borosilicate Glass

A borosilicate glass workpiece is chosen for machining the holes. Four through holes are drilled on the workpiece, corresponding to voltage and frequency parameter values.

The machining time taken for the drilling completion is noted for each run to determine which factor has the most effect on the machining time of the through-hole drilling process. The ECDM process is used to drill through holes in the glass workpiece. The four holes drilled pertaining to the four trials are marked in Fig 5.1. The holes are seen to have associated thermal stress cracks in the HAZ. However, these cracks are not a major issue because the trial runs aim to determine whether spark voltage or frequency has a more pronounced impact on the machining time and to estimate the optimized value of the same. The electrolyte concentration (40% by weight of NaOH) is held constant throughout the drilling process.

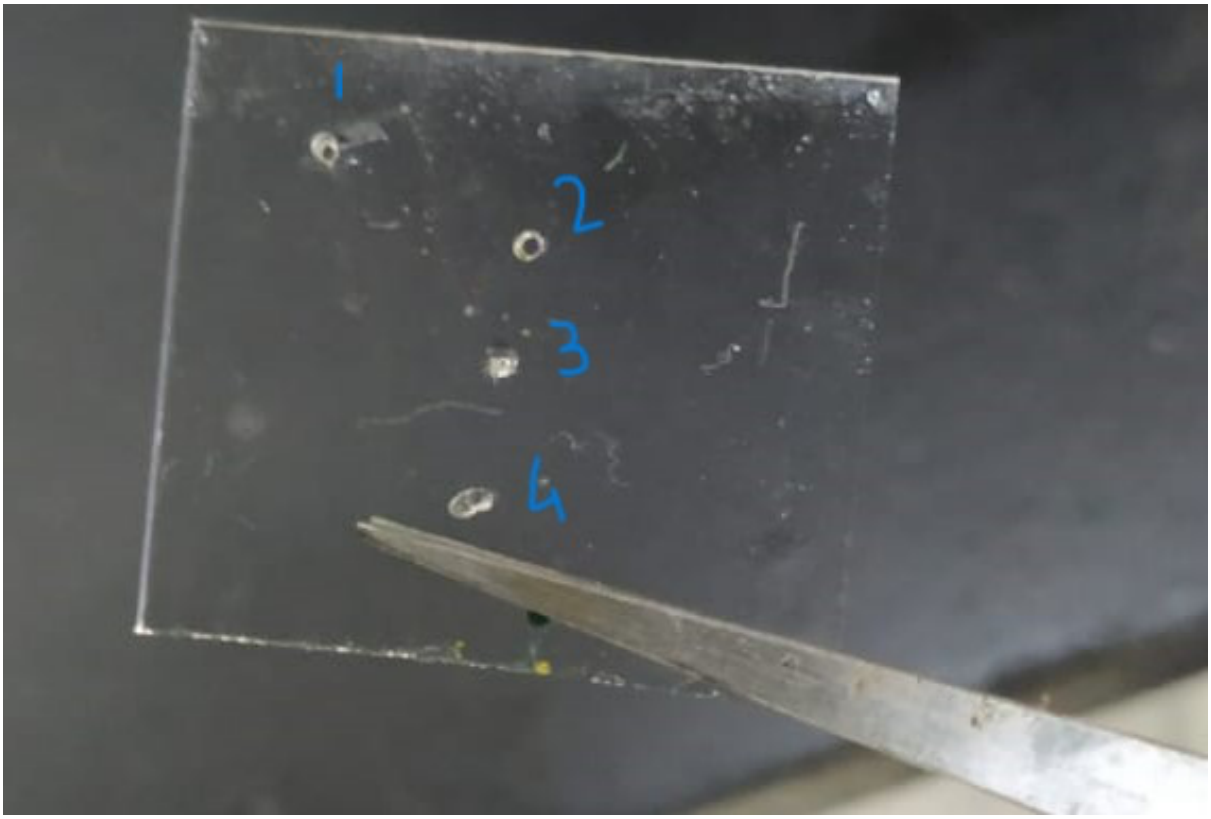

Fig 5.1 Closeup of borosilicate glass workpiece with through holes machined

Chapter 6: MINITAB Simulation and Cumulative Results

A higher R-squared indicates a better fit of the model to the data for regression models. Adjusted R-squared accounts for the number of predictors. They measure the proportion of variance in the response variable explained by the model, R-squared is the proportion explained, and adjusted R-squared considers the number of predictors. The model summary obtained in Minitab is shown in Fig 6.1.

Model Summary

S	R-sq	R-sq(adj)	R-sq(pred)
7.5	74.29%	22.86%	0.00%

Fig 6.1 Model Summary as obtained in Minitab

This table includes coefficients, standard errors, t-values, and p-values for each predictor variable in the model. It helps assess the significance and direction of the relationships. The coefficient table obtained is shown in Fig 6.2. The components are:

1. **Predictor Variables:**
    - The first column lists the predictor variables (independent variables) included in the regression model. Each row corresponds to a specific predictor.
2. **Coefficients (Estimates):**
    - The second column displays the estimated coefficients for each predictor variable. These coefficients represent the estimated change in the response variable for a one-unit change in the corresponding predictor, assuming all other variables are held constant.
3. **Standard Errors:**
    - The third column provides the standard errors associated with each coefficient estimate. Standard errors quantify the variability or precision of the coefficient estimates.
4. **T-Values:**

- The fourth column displays the t-values, which are calculated by dividing the coefficient estimate by its standard error. T-values help assess the statistical significance of each coefficient.

5. **P-Values:**

- The fifth column shows the p-values associated with each coefficient. P-values indicate the probability of observing a t-value as extreme as the one calculated, assuming the null hypothesis (no effect) is true. Low p-values suggest that the corresponding coefficient is statistically significant.

Coefficients

Term	Coef	SE Coef	T-Value	P-Value	VIF
Constant	18.75	3.75	5.00	0.126	
Voltage					
30	6.25	3.75	1.67	0.344	1.00
Frequency					
40	-1.25	3.75	-0.33	0.795	1.00

Fig 6.2 Coefficients obtained in Minitab

The regression equation obtained for the model is shown in Fig 6.3.

Regression Equation

Machining time = 18.75 + 6.25 Voltage_30 - 6.25 Voltage_60 - 1.25 Frequency_40
+ 1.25 Frequency_60

Fig 6.3 Regression equation obtained from MINITAB

The Pareto chart of the standardized effects obtained from the regression analysis is shown in Fig 6.4 as a part of the Design of Experiments (DoE). The bar graph shows that the voltage is the most significant factor influencing the machining time. This is also corroborated by experiments conducted on the in-house setup where varying the voltage shows drastic increases in Material Removal Rate (MRR) and reduced machining time. However, increasing a voltage

beyond a critical value does not necessarily augment the material removal. Increasing the voltage may also result in higher chances for the occurrence of cracks due to higher thermal stresses in the Heat Affected Zone (HAZ).

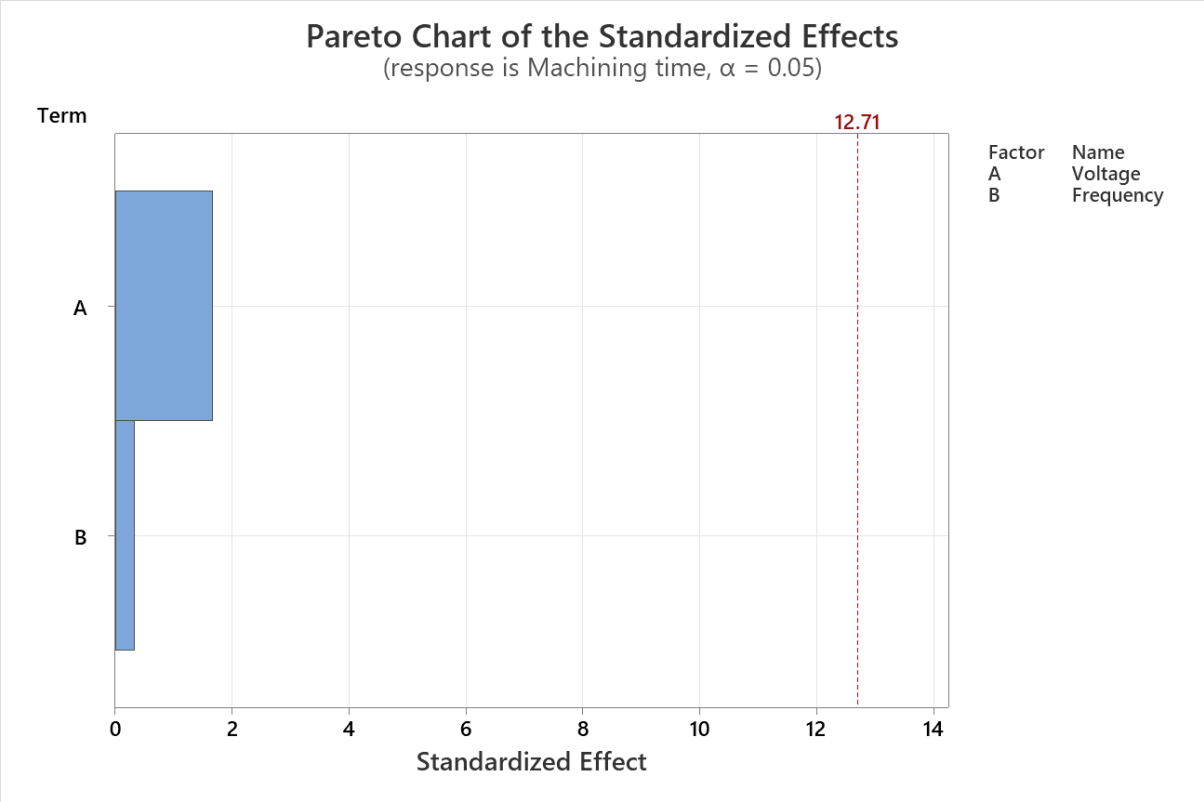

Fig 6.4 Pareto Chart of the Standardized Effects Obtained from Minitab

The residual plots obtained are shown in Fig 6.5. These are used to assess the validity of model assumptions and identify any patterns or outliers in the residuals. The types of residual plots are:

1. **Normal Probability Plot:**
    - This plot assesses the normality assumption of the residuals. Points on the plot should fall roughly along a straight line. Deviations from a straight line may indicate departures from normality.
2. **Residuals vs. Fitted Values Plot:**
    - This plot examines whether there is a systematic relationship between the residuals and the predicted values. Points should be randomly scattered around the horizontal axis.

3. **Residuals vs. Order Plot:**
    - This plot shows the residuals in the order in which they were collected. It helps identify patterns or trends in the residuals over time or experimental order.
4. **Residuals vs. Factors Plot:**
    - This plot displays residuals against the levels of the factors. It helps identify if there are any patterns or trends related to specific factor levels.

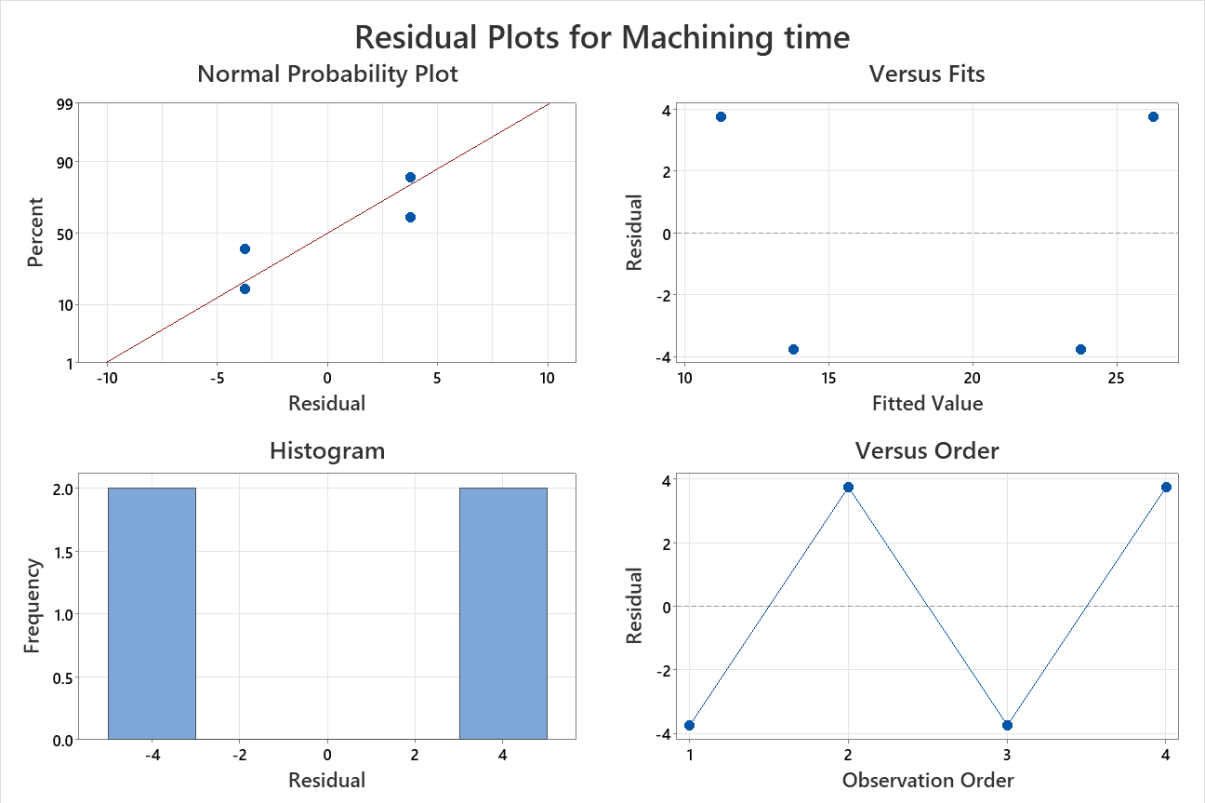

Fig 6.5 Machining Time Residual Plots obtained from Minitab

A main effects plot in Minitab is a graphical representation used in the context of factorial experiments to visualize the influence of individual factors on the response variable. It provides a clear illustration of the main effects of each factor, allowing researchers to assess the impact of varying factor levels on the response variable. This plot is shown in Fig 6.6. A steeper slope indicates that the corresponding factor has a stronger effect/impact. In this study the spark voltage is once again the dominant factor.

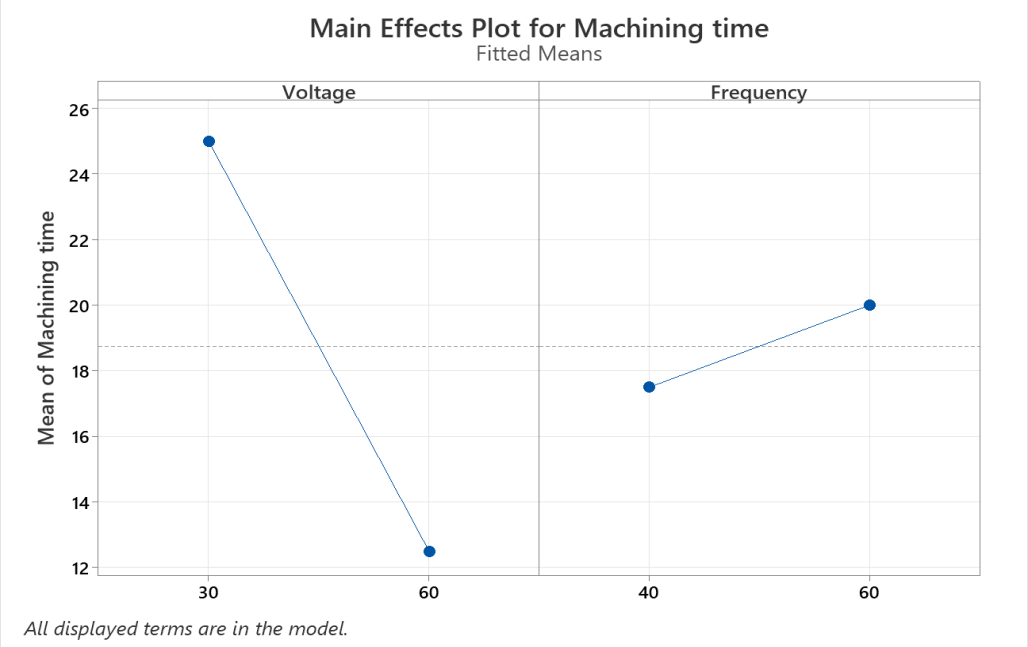

Fig 6.6 Main Effects Plot for Machining Time obtained from Minitab

The interaction plot for machining time is shown in Fig 6.7. The interaction plot generated in Minitab typically consists of separate line plots, each representing the levels of one factor, with lines for each level of the other factor. Since the lines cross, it indicates an interaction effect. The interaction plot shows that the optimal voltage is 52 V, and the corresponding machining time is 17.5 minutes.

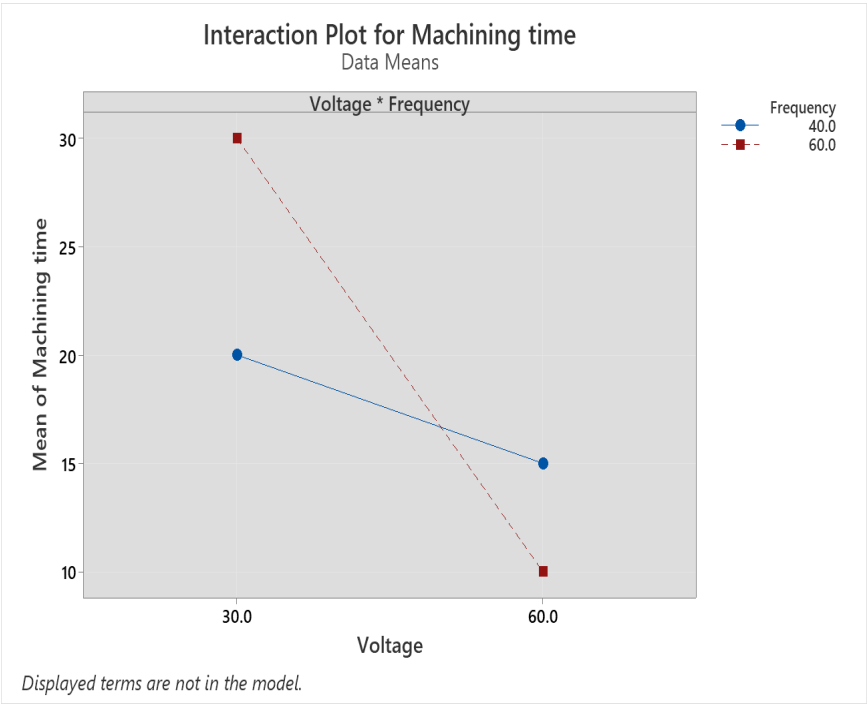

Fig 6.7 Interaction Plot for Machining Time in Minitab

6.1. Overview of Results

- Multi-level design is chosen with two levels and two factors each.
- Voltage and frequency are chosen as the factors.
- Four runs are carried out, and the ANOVA chart is generated. The plots are generated for the individual and the interaction effects of the two factors.
- It is observed that voltage affects and influences the overall machining time more than frequency. Hence, the experiment is more sensitive to changes in the voltage of the process.
- From the interaction plot, it is seen that the optimal voltage is 52 V, and the corresponding machining time is 17.5 minutes.

Reading References

1. Allesu, K., (1988): Electrochemical discharge phenomena in manufacturing process. Ph.D. Thesis, Indian Institute of Technology-Kanpur.
2. Al-Saedi, I. R. K., F. M. Mohammed and S. S. Obayes, (2017): CNC machine based on embedded wireless and Internet of Things for workshop development. International Conference on Control, Automation and Diagnosis (ICCAD), pp. 439-444, DOI: 10.1109/CADIAG.2017.8075699.
3. Basak, I., A. Ghosh, (1996): Mechanism of spark generation during electrochemical discharge machining: a theoretical model and experimental verification. Journal of Material Processing Technology 62, 46–53.
4. Ghosh, A., M. K. Muju, S. Parija, K. Allesu, (1997): Microwelding using electrochemical discharge. International Journal of Machine Tools and Manufacture 37, 1303–1312.
5. Hajian M, Razfar MR, Movahed Saeid, (2016): An experimental study on the effect of magnetic field orientations and electrolyte concentrations on ECDM milling performance of glass. Precision Engineering 45, 322-331.
6. Jain, V.K., P.M. Dixit, P.M. Pandey, (1999): On the analysis of the electrochemical spark machining process. International Journal of Machine Tools and Manufacture 39, 165–186.
7. Katsushi Furutani, Shunsuke Kojima, (2016): Prototyping of Acceleration Sensor by Using Lathe-type Electro-chemical Discharge Machine. Procedia CIRP, Volume 42, pp. 772-777, ISSN 2212-8271.
8. Kulkarni, A., R. Sharan, G.K. Lal, (2002): An experimental study of discharge mechanism in electrochemical discharge machining. International Journal of Machine Tools and Manufacture 42, 1121–1127.
9. Krotz Harry, Konrad Wegener, (2015): Sparc assisted electrochemical machining: a novel possibility for micro drilling into electrical conductive

materials using the electrochemical discharge phenomenon. International Journal of Advanced Manufacturing Technology DOI: 10.1007/s00170-015-6913-9.

10. Lijo Paul, Somashekhar S. Hiremath, (2016): Experimental and Theoretical Investigations in ECDM Process – An Overview. Procedia Technology, Volume 25, ISSN 2212-0173.
11. Siddhartha, B., A. P. Chavan, G. K. HD and K. N. Subramanya, (2020): IoT Enabled Real-Time Availability and Condition Monitoring of CNC Machines. IEEE International Conference on Internet of Things and Intelligence System (IoTaIS), pp. 78-84, DOI: 10.1109/IoTaIS50849.2021.9359698.
12. Vijayakumar, D. M. N., M. S. Archana and W. Kamalakant, (2018): Exploratory Study On The Application Of IoT In CNC. 3rd International Conference on Computational Systems and Information Technology for Sustainable Solutions (CSITSS), pp. 329-332, DOI: 10.1109/CSITSS.2018.8768502.
13. Mohan Krishna K., P. Kannadaguli, (2020): IoT Based CNC Machine Condition Monitoring System Using Machine Learning Techniques. IEEE 9th International Conference on Communication Systems and Network Technologies (CSNT), pp. 61-65, DOI: 10.1109/CSNT48778.2020.9115762.
14. Wansheng Zhao, Mo Chen, Weiwen Xia, Xuecheng Xi, Fuchun Zhao, Yaou Zhang, (2020): Reconstructing CNC platform for EDM machines towards smart manufacturing. Procedia CIRP, Volume 95, pp. 161-177, ISSN 2212-8271.
15. Yahya Mohammed Al-Naggar, Norlida Jamil, Mohd Firdaus Hassan, Ahmad Razlan Yusoff, (2021): Condition monitoring based on IoT for predictive maintenance of CNC machines. Procedia CIRP, Volume 102, pp. 314-318, ISSN 2212-8271.